AIP | Applied Physics Letters

Electrothermal phenomena in zinc oxide nanowires and contacts

Saniya LeBlanc, Sujay Phadke, Takashi Kodama, Alberto Salleo, and Kenneth E. Goodson

Citation: Appl. Phys. Lett. **100**, 163105 (2012); doi: 10.1063/1.4703935
View online: http://dx.doi.org/10.1063/1.4703935
View Table of Contents: http://apl.aip.org/resource/1/APPLAB/v100/i16
Published by the American Institute of Physics.

Electrothermal phenomena in zinc oxide nanowires and contacts

Saniya LeBlanc,[1] Sujay Phadke,[1] Takashi Kodama,[1] Alberto Salleo,[2] and Kenneth E. Goodson[1]
[1]*Department of Mechanical Engineering, Stanford University, Stanford, California 94305, USA*
[2]*Department of Materials Science and Engineering, Stanford University, Stanford, California 94305, USA*

(Received 6 March 2012; accepted 30 March 2012; published online 16 April 2012)

Heat generation along nanowires and near their electrical contacts influences the feasibility of energy conversion devices. This work presents ZnO nanowire electrical resistivity data and models electrothermal transport accounting for heat generation at metal-semiconductor contacts, axial thermal conduction, and substrate heat losses. The current-voltage relationships and electron microscopy indicate that sample degradation is caused by the interplay of heat generation at contacts and within the nanowire volume. The model is used to interpret literature data for Si, GaN, and ZnO nanowires. This work assists with electrothermal nanowire measurements and highlights practical implications of utilizing solution-synthesized nanowires. © *2012 American Institute of Physics*. [http://dx.doi.org/10.1063/1.4703935]

Nanowires are promising for applications including transistors,[1,2] sensors,[3,4] and energy conversion devices.[5] Recent research examined their potential in energy applications including thermoelectric waste heat recovery,[6,7] solar cells,[8] and batteries.[9–11] Zinc oxide nanostructures have generated particular interest due to their optical and electrical properties, ease of synthesis, and non-toxicity.[12–14] Most ZnO nanowire devices use electrical contacts where the contact composition and transport of energy carriers are critical for performance.[15] Contacts can dominate nanowire device response, particularly in devices exhibiting rectifying behavior.[16,17]

Nanoscale thermal contact resistance has been studied for nanowires and nanotubes. Using a contact resistance model based on acoustic mismatch theory,[18] the thermal resistance of a nanowire point contact and variations in phonon transmission through welded and non-welded nanowire contacts were determined for indium arsenide nanowires.[19] Heat generation and thermal failure limit the reliability of nanowire/nanotube devices.[20,21] Heat generation and electrical breakdown studies on individual carbon nanotubes show failure often occurs in the interior, away from contacts.[21] There is a pressing need for a methodology, determining the impact of heat generation in nanowire devices, particularly those which may have limited electrode contact area and interfacial layers. The need is significant for oxide nanowires such as ZnO, SnO_2, and MgO in which the nanocontact interfacial effects increase the effective contact resistance.[22]

This work analyzes heat generation within a nanowire and at its contacts, and the relative heat generation is used to determine nanowire device limitations. The model is applied to ZnO nanowires fabricated here using solution-synthesis.[23] Data for ZnO, GaN, and Si nanowire structures measured by other researchers are utilized to determine the relative heat generation for a broader range of materials.

The model considers a nanowire contacted by two metal electrodes as shown in Figure 1(a) with current flowing through the structure. The simplified one-dimensional heat diffusion equation

$$k_w A \frac{d^2T}{dx^2} + \rho_w A J^2 - g(T - T_o) = 0 \tag{1}$$

neglects the temperature dependence of both thermal conductivity and thermal conductance from the nanowire to the substrate. The parameters k_w, ρ_w, A, and T are the nanowire

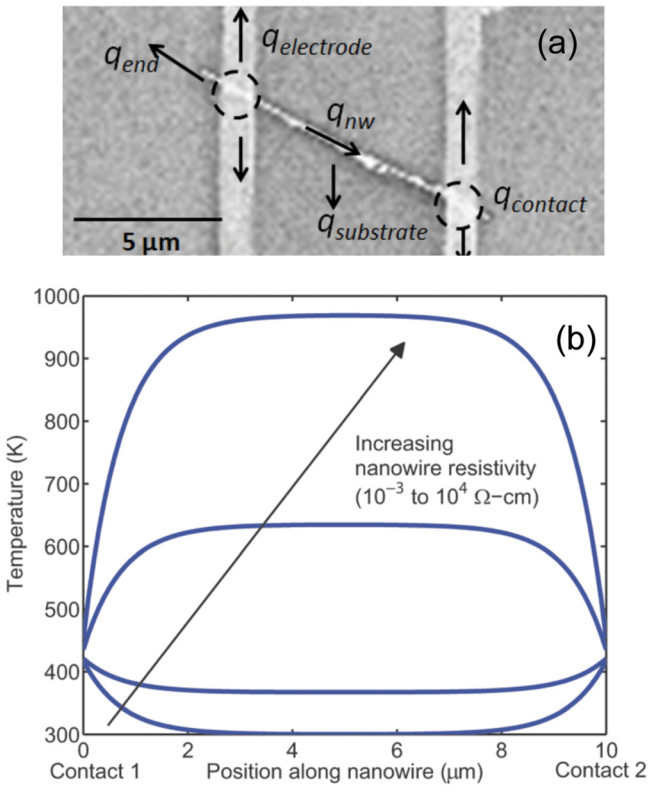

FIG. 1. (a) Scanning electron micrograph of a nanowire device with labels indicating heat conduction and generation. Metal-nanowire contacts are circled. (b) Temperature profiles obtained by applying the electrothermal analysis to a ZnO nanowire structure with metal contacts. The parameters used to generate the profiles are $k = 20$ W/m-K, $r = 80$ nm, $L_w = 10$ μm, $\rho_c = 5 \times 10^{-3}$ Ω-cm^2, $g = 1.2$ W/m-K, and $I = 400$ nA. The resistivity range is representative of ZnO nanowires measured by other researchers.[26]

thermal conductivity, resistivity, cross-sectional area, and local temperature, respectively. The first term quantifies heat diffusion along the nanowire; the second term accounts for Joule heating within the nanowire due to current density J flowing through it. Thermal boundary conductance g is used to calculate the rate of heat loss per unit length to the underlying substrate at ambient temperature T_o. By linearizing the relationship between the nanowire-substrate heat conduction with respect to the temperature difference, this analysis may overestimate the peak temperature distribution in the nanowire by up to 15% for temperature differences exceeding 1000 K. Other complications reduce the accuracy for the case of extreme temperature differences, including the temperature dependent thermal conductivity and nanowire-metal electrical and thermal contact resistances, which renders this approach approximate and best suited for scaling assessment. One-dimensional conduction is assumed, and temperature variations in the nanowire and electrode cross-sections are neglected. The resistance to heat conduction inside the nanowire and electrode cross-sections is several orders of magnitude smaller than the thermal resistance of their surroundings, so the 1D approximation is valid.[24]

Heat generation occurs at the electrode-nanowire contact due to electrical contact resistance. The model is applied to Ohmic contacts in which the metal work function is smaller than the semiconducting nanowire electron affinity, and the current-voltage relationship is linear. This condition does not preclude analysis of metal-nanowire contacts with interfacial layers so long as the barrier width is thin enough to fulfill the Ohmic contact requirement. The representation of electrical contact resistance for Schottky contacts[25] is not valid in this approach because it applies only near zero bias condition and does not describe the barrier to charge carrier transport resulting in heat generation.

Research on thermal contact resistance between a nanowire and an underlying substrate provided a theoretical framework for determining this thermal resistance based on van der Waals interactions between the two surfaces.[27] An extended model accounting for ballistic and diffusive phonon transport through a nanoscale constriction was developed along with the effective reduction in fluid thermal conductivity due to the small gap between the nanowire and substrate.[28] Both approaches have been applied to experimental characterization of a carbon nanotube with the extended model predicting a value closer to the one deduced from experiments.[29] The phonon mean free path in ZnO is approximately 30 nm; the contact width between the nanowire and substrate is 2 nm for nanowires analyzed here. While the contact is smaller than the phonon mean free path, the substrate is a 200 nm layer of SiO_2 on silicon, so transport across the interface is treated as diffusive. Thermal constriction resistance R_c to a substrate with thermal conductivity k_s is[27]

$$R_c = \frac{1}{L_w}\left[\frac{1}{\pi k_w}\ln\left(\frac{2D}{w}\right) - \frac{1}{2k_w} + \frac{1}{\pi k_s}\ln\left(\frac{D}{\pi w}\right)\right], \quad (2)$$

where L_w, D, and w are the nanowire length, diameter, and the half-width of its contact with the substrate, respectively. The effective thermal resistance R_f of the fluidic gap between the nanowire and substrate is[28]

$$\frac{1}{R_f} = 2L_w k_f \int_w^{D/2} \frac{dy}{D/2 - \sqrt{D^2/4 - y^2} + 2a\lambda_f}, \quad (3)$$

where a is 2 for an air gap at room temperature, k_f is the thermal conductivity of the fluid, and λ_f is the mean free path of air molecules. The total thermal resistance R_t is $R_t = (R_c R_f)/(R_c + R_f)$. The heat loss g is the inverse of this thermal resistance divided by nanowire length.

The model yields the temperature profile of a nanowire with contacting electrodes. Figure 1(b) demonstrates the results for a nanowire device where symmetric contact heat generation is assumed. Asymmetric contact heating could occur in rectifying systems with Ohmic and Schottky contacts. The temperature distribution depends strongly on nanowire electrical resistance as demonstrated by the case where the large nanowire resistivity leads to a peak device temperature within the nanowire. Several researchers have conducted experiments using the resulting nanowire/nanotube failure to characterize the nanostructure's properties.[20,30] Nonetheless, there is another critical failure mode in which metal-nanowire contact resistance dominates.

The electrothermal model is applied to measurement structures of 1% Ga-doped ZnO nanowires with Ti/Ag electrodes. The nanowires were solution-synthesized and single crystalline wurtzite in structure.[23] A dilute nanowire solution was dispersed on a silicon substrate topped with 200 nm SiO_2. Electrodes were patterned on nanowires with electron beam lithography as shown in Figure 2; atomic force microscopy was used to verify electrode thickness. Images obtained with an FEI XL30 Sirion scanning electron microscope (SEM) enabled extraction of nanowire and electrode dimensions. A Keithley 2612 measured current and voltage to provide electrical resistance.

A transmission line analysis yields specific contact resistivity of the metal-nanowire contact.[31–33] The electrical contact resistance R_m between the metal and the nanowire is[31,33]

$$R_m = \frac{\rho_c}{2\pi L_T F}\coth\frac{L_m}{L_T}, \quad (4)$$

L_T, the electrical transfer length[31,33]

$$L_T = \sqrt{\frac{r\rho_c}{2F\rho_w}} \quad (5)$$

relates nanowire resistivity ρ_w to specific resistivity of the metal-nanowire contact ρ_c. The fraction of nanowire

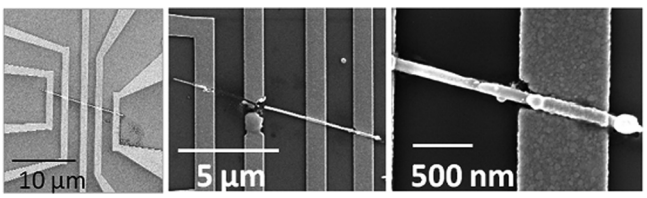

FIG. 2. Scanning electron microscope image of ZnO nanowire device (a) before and (b) and (c) after measurement. There is pitting of the contact where the effective electrode width and area of contact with the nanowire decrease, and the metal electrode melts. The rightmost electrode shown in (a) was not used for measurements presented here.

TABLE I. ZnO nanowire parameters determined here from 4- and 2-point measurements.

Sample	r (nm)	ρ_w (Ω-cm)	ρ_c (Ω-cm^2)
1	52	4.7×10^{-3} ($\pm 2.4 \times 10^{-3}$)	5.4×10^{-4} ($\pm 1.3 \times 10^{-4}$)
2	67	1.0×10^{-2} ($\pm 1.4 \times 10^{-2}$)	17 ($\pm$12)

circumference covered by metal is F for a nanowire with radius r; the length of contact is L_m. SEM imaging of the structures tilted at various angles show the majority (~75% or more) of the nanowire circumference is covered by metal. Full coverage ($F = 1$) is assumed, providing an upper-bound on ρ_c. The total resistance between two contacts is $R_T = 2R_m + (\rho_w/\pi r^2)L_w$. A 4-point measurement reveals nanowire resistivity, which is used with 2-point measurements to determine contact resistance. Surface depletion is neglected; the analysis assumes the entire nanowire cross-section is used for electrical conduction. This assumption is validated by a calculation of the depletion width which is less than 3 nm, less than 5% of the radius.[34]

Nanowire and specific contact resistivity for two structures are listed in Table I. There are two possible reasons the extracted contact resistivity spans multiple orders of magnitude. Solution-synthesized nanowires often have a surfactant coating remaining on the nanowire surface. Raman spectroscopy on the same batch of nanowires measured here shows evidence of the surfactant.[35] Multiple 4-point measurements were performed on sample 2 before the 2-point measurements. It is possible one of the electrode-nanowire contact areas decreased during the measurement. In this case, the actual contact resistivity would be lower than the value calculated using the contact area determined from pre-measurement SEM images.

Incorporating experimental nanowire and contact resistivity values into the electrothermal model indicates the peak temperature rise occurs at the metal-nanowire contact. At the maximum measured current of 5 μA, the predicted contact temperature is 900 K, which approaches the silver electrode melting point. Shown in Figure 2, post-measurement images show device failure at the metal contact while much of the nanowire between the electrodes remains intact. The images reveal pitting of the metal at the contact, resulting in reduced contact area between the nanowire and electrode. The pitting may be due to current crowding at the leading edge of the metal-nanowire contact region.[36] The localized region of high current density at the leading edge may exacerbate electromigration of the metal electrode. Therefore, the actual contact area between the electrode and nanowire is less than the nominal value causing an increase in current density and contact temperature as shown in Figure 3. Failure of the device occurs at one contact, indicating the contact resistances are asymmetric. Though challenging due to the rapid evolution of dimensional changes from heat generation, an informative future study would involve *in situ* imaging of the nanowire structure during the electrical measurement to capture the dynamic change in electrode width.

Analysis of nanowire structure failure is critical to the development of reliable devices. It is useful to compare heat generation in the nanowire divided by heat generation at the contacts. For Ohmic contacts and device current I, this non-

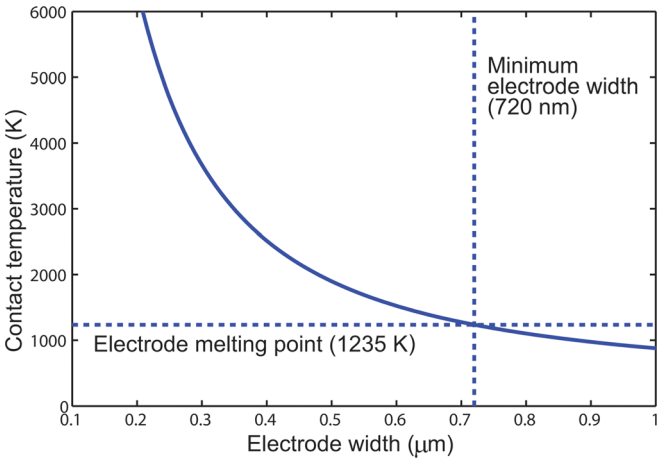

FIG. 3. Peak contact temperature changes with electrode width. The minimum width the ZnO nanowire device can tolerate is 720 nm; further electrode narrowing causes the contact to reach the electrode melting point.

dimensional relative heat generation is represented as $\theta = I^2R_w/(I\Pi + I^2R_w)$, which can also be expressed as

$$\theta = \frac{J\rho_w L_w}{\pm\frac{1}{e}[(E_C - E_F) + Ck_bT] + J\rho_w L_T \coth(L_m/L_T)}, \quad (6)$$

where E_C and E_F are the semiconducting nanowire conduction band edge and Fermi level, respectively. The parameter C in the Peltier coefficient Π depends on the variation of the density of states and mobility with energy.[37] The numerator represents nanowire Joule heating. The denominator has two components contributing to contact heating, the Peltier effect and the power dissipated due to electrical contact resistance. The sign of the Peltier term depends on the direction of current through the metal-nanowire contact where one contact has a positive Peltier heat release term while the other has a negative heat absorption term. The relative heat generation θ thus indicates where nanowire device failure is likely. Figure 4 shows the relative heating as a function of contact resistivity for the wide range of ZnO nanowire contact resistivity.[26] As

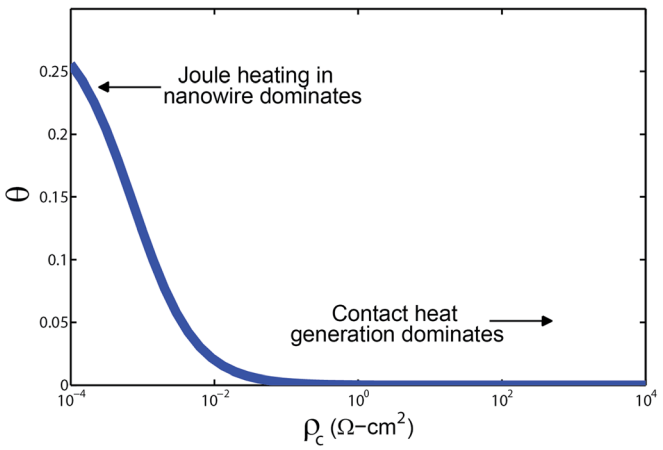

FIG. 4. Ratio, θ, of the heat generation rate in the nanowire to the heat generation at the contacts varies with electrical contact resistivity of the metal-nanowire contact and indicates the likely device failure point. The figure shows the variation in θ for a ZnO nanowire device operating at 1 μA for which the Peltier coefficient is evaluated at the contact temperature determined from the electrothermal model. The parameters used are $\Pi = 0.17$ V, $r = 66$ nm, $L_w = 7$ μm, $\rho_w = 1 \times 10^{-2}$ Ω-cm.

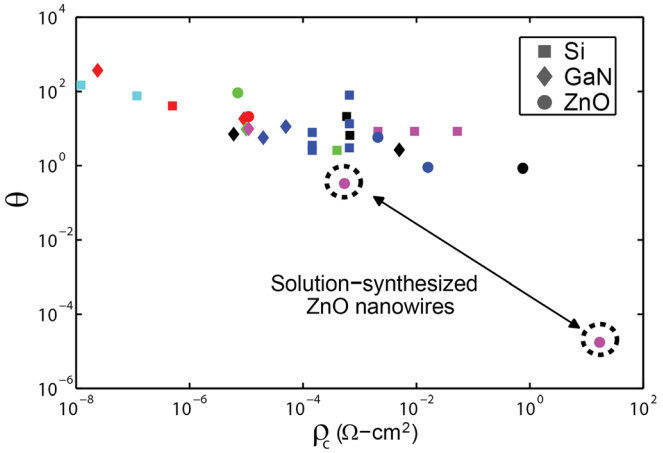

FIG. 5. The ratio of nanowire-internal to contact heat generation plotted as a function of reported contact resistivity for Si (■), GaN (◆), and ZnO (●) nanowire devices from various studies (Si,[31,38–42] GaN,[33,43–46] ZnO[2,47–49]). Nanowire material type is designated by marker type. Data from each source are differentiated by color as indicated in the references. Data from this work are circled.

effective contact resistance of the junction increases, or nanowire resistivity decreases, the device is more prone to fail at the contact.

Electrothermal transport data for relevant materials are examined to assess the impact of relative heating on an array of nanowire devices proposed for energy conversion applications. Figure 5 shows the relative heating versus specific contact resistivity for silicon,[31,38–42] gallium nitride,[33,43–46] and zinc oxide.[2,47–49] Using data reported by previous studies, the relative heat generation rate is determined assuming typical metal-nanowire contact length, nanowire length, and device current of 1 μm, 10 μm, and 1 μA, respectively. The electrical transfer length is calculated assuming full metal coverage ($F = 1$). When not reported, nanowire radius is measured from the authors' presented SEM images using an image analysis program. If authors report carrier concentration and mobility from 4-point measurements, nanowire resistivity is calculated. The Peltier term is several orders of magnitude less than heating from contact resistivity, so this term was neglected in calculations for the data in Figure 5.

The comparison of multiple nanowire devices demonstrates a wide range of specific contact resistivity, approximately 1.2×10^{-8} to 0.75 Ω-cm^2. Likewise, the relative heating parameter for devices other than the solution-synthesized ZnO nanowires spans two orders of magnitude. ZnO nanowire structures with relative heating parameters below 0.1 where contact heating dominates will likely fail during device operation due to melting of the metal contact. Little information is reported for such failures, rendering a thorough analysis of experimental electrothermal phenomena in nanowire devices difficult. The necessity of such communication is highlighted by this analysis. The paucity of such data for solution-synthesized nanowires is significant. With the exception of data reported here for ZnO, the data used to generate Figure 5 are taken from measurements of vapor-synthesized (e.g., chemical vapor deposition, vapor-liquid-solid growth) nanowires. Ease of fabrication makes solution-synthesized nanowires promising, but contact resistivity may limit their functionality and impact device performance. Annealing processes to eliminate residual surfactant are particularly limited with ZnO nanowires since an insulating oxide readily forms at the nanowire-metal contact for multiple metals, a process that can be amplified with elevated temperatures. Annealing of these solution-synthesized ZnO nanowire structures with Ti and Ti/Al electrodes showed a reduction in electrical conductivity.

This work proposes an electrothermal model, which links current-voltage measurement data to the resulting temperature profile of semiconducting ZnO nanowire devices. The contact resistance of the metal-semiconductor contact leads to heat generation at the contact, which surpasses the nanowire Joule heating. Therefore, the contact heat generation limits the operating range of the nanowire device. This approach is used to determine design and operating parameters for nanowire devices. Additionally, recent reviews demonstrate the substantial variability in ZnO nanowire devices, particularly at the metal-semiconductor contacts. This work highlights the significance of these contacts and the need for further contact characterization and improvements.

This work was supported by Sandia National Laboratories, National Science Foundation Graduate Research, and Stanford DARE fellowships, as well as an NSF/DOE Partnership on Thermoelectric Devices for Vehicle Applications grant.

[1]J.-P. Colinge, C.-W. Lee, A. Afzalian, N. D. Akhavan, R. Yan, I. Ferain, P. Razavi, B. O'Neil, A. Blake, M. White, A.-M. Kelleher, B. McCarthy, and R. Murphy, Nat. Nanotechnol. **5**, 225–229 (2010).
[2]J. Goldberger, D. J. Sirbuly, M. Law, and P. Yang, J. Phys. Chem. B **109**, 9–14 (2005). (Data from this source used for Figure 5, blue circles.)
[3]F. Patolsky and C. M. Lieber, Mater. Today **8**(4), 20–28 (2005).
[4]A. Menzel, K. Subannajui, F. Guder, D. Moser, O. Paul, and M. Zacharias, Adv. Funct. Mater. **21**, 4342–4348 (2011).
[5]A. I. Hochbaum and P. Yang, Chem. Rev. **110**, 527–546 (2010).
[6]S. C. Andrews, M. A. Fardy, M. C. Moore, S. Aloni, M. Zhang, V. Radmilovic, and P. Yang, Chem. Sci. **2**, 706–714 (2011).
[7]J. A. Martinez, P. P. Provencio, S. T. Picraux, J. P. Sullivan, and B. S. Swartzentruber, J. Appl. Phys. **110**, 074317 (2011).
[8]E. C. Garnett, M. L. Brongersma, Y. Cui, and M. D. McGehee, Annu. Rev. Mater. Res. **41**, 269–295 (2011).
[9]C. K. Chan, R. N. Patel, M. J. O'Connell, B. A. Korgel, and Y. Cui, ACS Nano **4**, 1443–1450 (2010).
[10]S. R. Gowda, A. L. M. Reddy, X. Zhan, and P. M. Ajayan, Nano Lett. **11**, 3329–3333 (2011).
[11]C. K. Chan, H. Peng, G. Liu, K. McIlwrath, X. F. Zhang, R. A. Huggins, and Y. Cui, Nat. Nanotechnol. **3**, 31–35 (2008).
[12]U. Ozgur, Y. I. Alivov, A. Teke, M. A. Reshchikov, S. Dogan, V. Avrutin, S.-J. Cho, and H. Morkoc, J. Appl. Phys. **98**, 041301 (2005).
[13]A. B. Djurisic, X. Chen, Y. H. Leung, and A. M. C. Ng, J. Mater. Chem. **22**, 6526–6535 (2012).
[14]P. Jood, R. J. Mehta, Y. Zhang, G. Peleckis, X. Wang, R. W. Siegel, T. Borca-Tasciuc, S. X. Dou, and G. Ramanath, Nano Lett. **11**, 4337–4342 (2011).
[15]L. J. Brillson and Y. Lu, J. Appl. Phys. **109**, 121301 (2011).
[16]Z. Zhang, K. Yao, Y. Liu, C. Jin, X. Liang, Q. Chen, and L.-M. Peng, Adv. Funct. Mater. **17**, 2478–2489 (2007).
[17]Y.-F. Lin and W.-B. Jian, Nano Lett. **8**, 3146–3150 (2008).
[18]R. Prasher, Appl. Phys. Lett. **94**, 041905 (2009).
[19]F. Zhou, A. Persson, L. Samuelson, H. Linke, and L. Shi, Appl. Phys. Lett. **99**, 063110 (2011).
[20]T. Westover, R. Jones, J. Y. Huang, G. Wang, E. Lai, and A. A. Talin, Nano Lett. **9**, 257–263 (2009).
[21]A. Liao, R. Alizadegan, Z.-Y. Ong, S. Dutta, F. Xiong, K. J. Hsia, and E. Pop, Phys. Rev. B **82**, 205406 (2010).
[22]K. Nagashima, T. Yanagida, A. Klamchuen, M. Kanai, K. Oka, S. Seki, and T. Kawai, Appl. Phys. Lett. **96**, 073110 (2010).

[23]L. Goris, R. Noriega, M. Donovan, J. Jokisaari, G. Kusinski, and A. Salleo, J. Electron. Mater. **38**, 586–595 (2009).
[24]F. P. Incropera, *Fundamentals of Mass and Heat Transfer* (McGraw-Hill, New York, 2007).
[25]S. M. Sze and K. K. Ng, *Physics of Semiconductor Devices*, 3 ed. (Wiley-Interscience, Hoboken, NJ, 2007).
[26]E. Schlenker, A. Bakin, T. Weimann, P. Hinze, D. H. Weber, A. Golzhauser, H.-H. Wehmann, and A. Waag, Nanotechnology **19**, 365707 (2008).
[27]V. Bahadur, J. Xu, Y. Liu, and T. S. Fisher, J. Heat Transfer **127**, 664 (2005).
[28]R. Prasher, Nano Lett. **5**, 2155–2159 (2005).
[29]C. Yu, S. Saha, J. Zhou, L. Shi, A. M. Cassell, B. A. Cruden, Q. Ngo, and J. Li, J. Heat Transfer **128**, 234–239 (2006).
[30]E. Pop, D. A. Mann, K. E. Goodson, and H. Dai, J. Appl. Phys. **101**, 093710 (2007).
[31]S. E. Mohney, Y. Wang, M. A. Cabassi, K. K. Lew, S. Dey, J. M. Redwing, and T. S. Mayer, Solid State Electron. **49**, 227–232 (2005). (Data from this source used for Figure 5, black squares.)
[32]H. H. Berger, Solid State Electron. **15**, 145–158 (1972).
[33]L. M. Mansfield, K. A. Bertness, P. T. Blanchard, T. E. Harvey, A. W. Sanders, and N. A. Sanford, J. Electron. Mater. **38**, 495–504 (2009). (Data from this source used for Figure 5, green diamond.)
[34]B. S. Simpkins, M. A. Mastro, C. R. Eddy, and P. E. Pehrsson, J. Appl. Phys. **103**, 104313 (2008).
[35]S. A. Phadke, Y. Park, F. B. Prinz, and A. Salleo, "A Study of the Cause of High Nanowire to Nanowire Junction Resistance in Conducting ZnO Nanowire Mats" (unpublished).
[36]K. L. Grosse, M.-H. Bae, F. Lian, E. Pop, and W. P. King, Nat. Nanotechnol. **6**, 287–290 (2011).
[37]H. Fritzsche, Solid State Commun. **9**, 1813–1815 (1971).
[38]I. Park, Z. Li, A. P. Pisano, and R. S. Williams, Nanotechnology **21**, 015501 (2010). (Data from this source used for Figure 5, blue squares.)
[39]M. T. Björk, H. Schmid, J. Knoch, H. Riel, and W. Riess, Nat. Nanotechnol. **4**, 103–107 (2009). (Data from this source used for Figure 5, red square.)
[40]H. D. Tong, S. Chen, W. G. van der Wiel, E. T. Carlen, and A. van den Berg, Nano Lett. **9**, 1015–1022 (2009). (Data from this source used for Figure 5, green squares.)
[41]K.-K. Lew, L. Pan, T. E. Bogart, S. M. Dilts, E. C. Dickey, J. M. Redwing, Y. Wang, M. Cabassi, T. S. Mayer, and S. W. Novak, Appl. Phys. Lett. **85**, 3101 (2004). (Data from this source used for Figure 5, magenta squares.)
[42]S. Habicht, Q. T. Zhao, S. F. Feste, L. Knoll, S. Trellenkamp, B. Ghyselen, and S. Mantl, Nanotechnology **21**, 105701 (2010). (Data from this source used for Figure 5, cyan squares.)
[43]E. Stern, G. Cheng, M. P. Young, and M. A. Reed, Appl. Phys. Lett. **88**, 053106 (2006). (Data from this source used for Figure 5, black diamonds.)
[44]A. Motayed, A. V. Davydov, S. N. Mohammad, and J. Melngailis, J. Appl. Phys. **104**, 024302 (2008). (Data from this source used for Figure 5, blue diamonds.)
[45]G. Ye, K. Shi, R. Burke, J. M. Redwing, and S. E. Mohney, J. Nanomater. **2011**, 876287 (2011). (Data from this source used for Figure 5, red diamonds.)
[46]C. Hwang, J.-H. Hyung, S.-Y. Lee, C.-O. Jang, T.-H. Kim, P. Choi, and S.-K. Lee, J. Phys. D **41**, 159802–159802 (2008). (Data from this source used for Figure 5, magenta diamonds.)
[47]T. Weimann, P. Hinze, E. Schlenker, A. Bakin, A. C. Mofor, A. Behrends, and A. Waag, Microelectron. Eng. **85**, 1248–1252 (2008). (Data from this source used for Figure 5, black circle.)
[48]J. H. He, P. H. Chang, C. Y. Chen, and K. T. Tsai, Nanotechnology **20**, 135701 (2009). (Data from this source used for Figure 5, red circle.)
[49]G.-D. Yuan, W.-J. Zhang, J.-S. Jie, X. Fan, J.-X. Tang, I. Shafiq, Z.-Z. Ye, C.-S. Lee, and S.-T. Lee, Adv. Mater. **20**, 168–173 (2008). (Data from this source used for Figure 5, green circle.)